Earth Planet. Sci. Lett. 645 (2024) 118952

Contents lists available at ScienceDirect

Earth and Planetary Science Letters

journal homepage: www.elsevier.com/locate/epsl

Partial melting of arclogite and petrogenesis of alkaline-silicate complexes

Emilie E. Bowman [a,*], Ananya Mallik [a], Mihai N. Ducea [b,a]

[a] Department of Geosciences, University of Arizona, 1040 E. 4th street, Tucson, AZ 85721, USA
[b] Faculty of Geology and Geophysics, University of Bucharest, Bucharest, 010040 Romania

ARTICLE INFO

Keywords:
Arclogite
Partial melting
Alkaline-silicate complex
Arc magmatism

ABSTRACT

Magmatic processing in the lower crust of thick-crusted (>40 km) arcs generates garnet-rich clinopyroxenite residues (arclogites) that are denser than the underlying mantle and therefore susceptible to foundering. Arclogites, which can contain substantial amphibole, may undergo partial melting as they sink into the subarc mantle. To constrain the geochemical composition of arclogite-derived melts and the role of arclogite in magmagenesis, we conducted partial melting experiments on average amphibole-bearing arclogite ARC15 at 2 GPa from 1040 to 1300 °C. At subsolidus conditions, garnet and clinopyroxene coexist with lesser amounts of amphibole, ilmenite, and biotite. Hydrous ARC15 begins melting between 1040 and 1080 °C. Once amphibole and biotite are exhausted by 1140 and 1190 °C, respectively, garnet becomes the primary melting phase according to the reaction 0.8 Garnet + 0.2 Clinopyroxene = 1 Melt. At 1300 °C, ARC15 yields 18 wt.% melt, indicating an anomalously low melt productivity of 0.12%/°C and rendering it the least melt-productive of all experimental pyroxenites investigated at 2 GPa. Geochemically, melts sourced from ARC15 are predominantly basanitic with low SiO_2 (43–52 wt.%) and high FeO (10–17 wt.%), TiO_2 (2.5–3.7 wt.%), and alkali ($Na_2O + K_2O$ = 3–6.5 wt.%) contents. Such compositions do not resemble magmas erupted at thick-crusted arcs, indicating that arclogites are not a dominant source of magmatism in these settings. Rather, the compositions of ARC15 melts more closely match those of magmas emplaced at post-collisional alkaline-silicate complexes, which form as a result of orogenic collapse and subsequent continental rifting and are common hosts of economic rare-earth element (REE) deposits. Trace element modeling further indicates derivation of alkaline-silicate magmas from variably metasomatized, light REE-enriched arclogite. Our results suggest a geodynamic model in which subduction beneath thickened crust leads to arclogite formation, foundering, and metasomatism as the material descends through the subduction-influenced mantle. During this stage, partial melts sourced from arclogite are likely modified by subduction-related secondary processes which dilute their diagnostic geochemical signatures. Subsequent collision and orogenic collapse induce extensional stresses that facilitate asthenospheric upwelling, leading to partial melting of the arclogite-bearing mantle and efficient extraction of primitive arclogite melts to the surface to form alkaline-silicate complexes and associated REE deposits.

1. Introduction

Arclogites, or garnet ± amphibole clinopyroxenites, are cumulates and restites that form during fractional crystallization and partial melting, respectively, in the near-Moho hot zone of thick-crusted (>40 km) arcs (Ducea et al., 2021a). These rocks are significant in that they have densities up to 10% greater than the underlying mantle, rendering them gravitationally unstable and subject to foundering (Lee, 2014; Bowman et al., 2021). Because they can contain up to 20 vol.% amphibole (Ducea et al., 2021a), arclogites may undergo dehydration melting as they descend into the hot core of the mantle wedge (Elkins-Tanton, 2007; Ducea et al., 2021b). If their solidus temperatures are sufficiently low, arclogites may even partially melt prior to detachment during their residence in the subarc lower crust. Arclogites may therefore be an important source of primary magmas, yet the geochemical composition of arclogite-derived melts as well as the contribution of arclogite melting to Earth's magmatic systems remains unconstrained.

Arclogites are silica-deficient (SD) garnet pyroxenites, distinguished from silica-excess (SE) garnet pyroxenites (e.g., eclogitized mid-ocean ridge basalt) by their higher forsterite and lower quartz components in the pseudoternary diagram forsterite–calcium Tschermak's pyroxene

* Corresponding author.
E-mail address: eebowman@arizona.edu (E.E. Bowman).

https://doi.org/10.1016/j.epsl.2024.118952
Received 27 December 2023; Received in revised form 29 July 2024; Accepted 14 August 2024

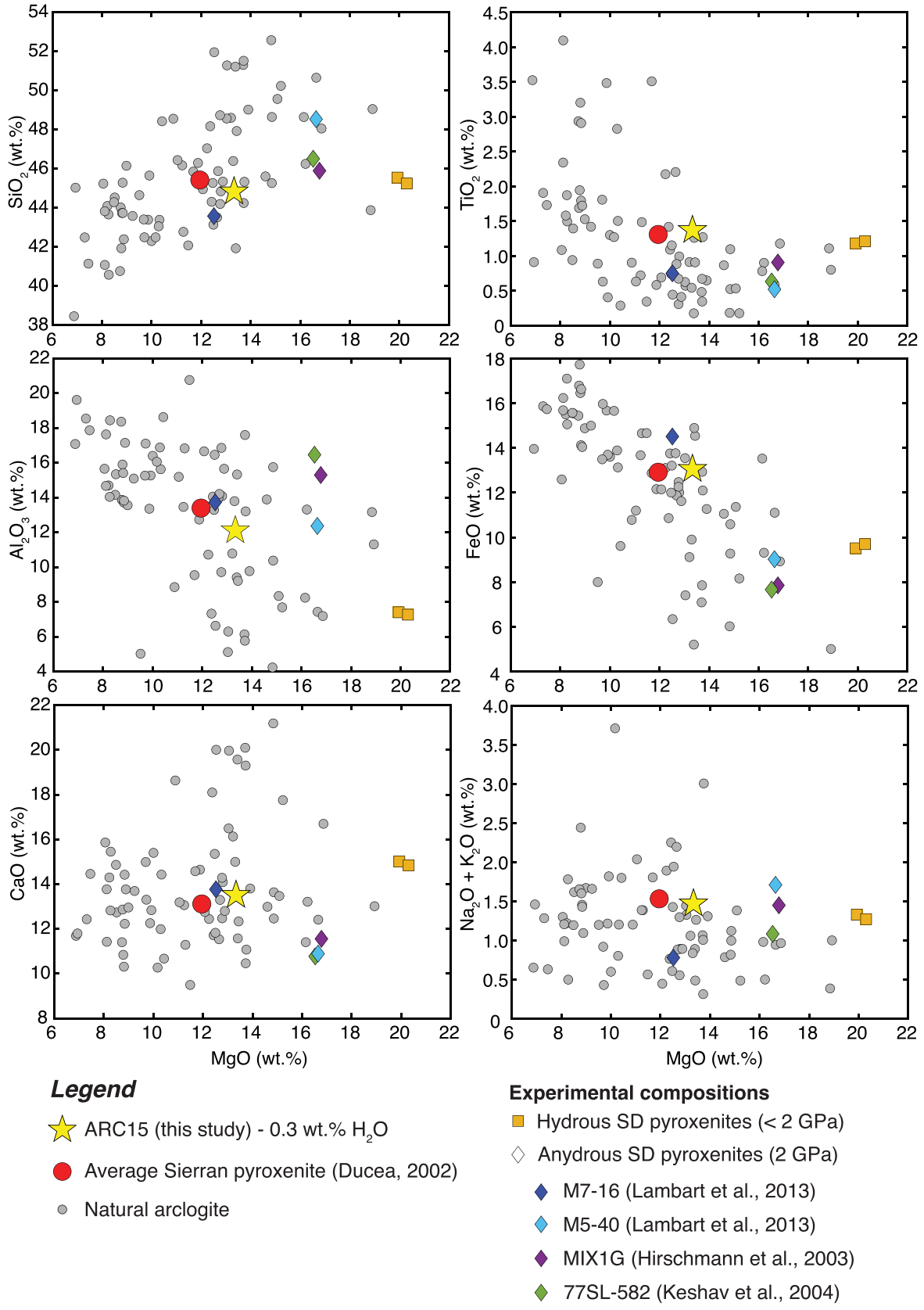

Fig. 1. Major element variation diagrams for the starting composition used in our experiments (ARC15) compared to average Sierran pyroxenite (Ducea, 2002) as well as other natural arclogites from the Sierra Nevada, Kohistan arc, Mercaderes, and Arizona arclogite localities (see Supplemental Materials for compilation of natural arclogite compositions and references). Also plotted are anhydrous and hydrous silica-deficient (SD) pyroxenites investigated in previously published experimental studies. Hydrous SD pyroxenite compositions plotted here are amphibole-bearing wehrlites (OCA2; Medard et al., 2006; Sorbadere et al., 2013). (For interpretation of the references to colour in this figure legend, the reader is referred to the web version of this article.)

Table 1
Major element composition (normalized to an anhydrous total of 100 wt.%) and H_2O content (wt.%) of starting material ARC15.

Starting composition	ARC15
SiO_2	44.83(26)
TiO_2	1.37(2)
Al_2O_3	12.11(9)
FeO	13.05(14)
MnO	0.25(2)
MgO	13.33(9)
CaO	13.51(4)
Na_2O	1.20(4)
K_2O	0.27(1)
P_2O_5	0.08(2)
Total	100
Mg#	0.65
H_2O	0.30

Major element composition is based on an average of 10 glass EPMA analyses. The cited H_2O content corresponds to that which was calculated from the addition of $Mg(OH)_2$ to the starting mixture. Numbers in parentheses are least unit cited 1σ errors calculated from replicate analyses, where 44.83(26) equates to 44.83 ± 0.26.

(CaTs)–quartz projected from diopside (Kogiso et al., 2004). In this system, a thermal divide along the enstatite-CaTs join becomes effective at pressures ≥ 2 GPa, causing melts derived from SE and SD garnet pyroxenites to evolve along different geochemical paths; as a result, SD pyroxenites yield magmas with consistently lower silica contents compared to SE pyroxenites (Lambart et al., 2013). Unfortunately, there is a lack of partial melting experiments on SD garnet pyroxenites, with even fewer investigating arclogitic compositions. For example, previous partial melting experiments on SD amphibole-bearing pyroxenite cumulates (OCA2; Medard et al., 2006; Sorbadere et al., 2013) were conducted at pressures too low to either stabilize garnet or destabilize plagioclase, and none of these experiments focus on starting compositions similar to that of average arclogite (Fig. 1). Moreover, all high-pressure (≥ 2 GPa) experiments on SD garnet clinopyroxenites have considered only anhydrous compositions, most of which are far too MgO-rich to represent average arclogite (MIX1G, Hirschmann et al., 2003; 77SL-582, Keshav et al., 2004; M5–40, Lambart et al., 2013). Only M7–16 (Lambart et al., 2013), a garnet-olivine clinopyroxenite, approximates the major element signature of anhydrous arclogite, yet like many of the published experiments, was studied at fO_2 conditions inconsistent with arc settings.

Nevertheless, limited compositional data do exist for arclogite melts. First-row transition element partitioning studies (Le Roux et al., 2010, 2011) indicate that magmas derived from garnet clinopyroxenites will have high Zn/Fe ratios compared to those sourced from peridotite, owing to the low (<1) mineral-melt $K_D^{Zn/Fe}$ of garnet and clinopyroxene relative to olivine and orthopyroxene. Zn/Fe ratios, however, cannot discriminate between the different types of garnet clinopyroxenites (e.g., eclogite vs. arclogite) that might be melting at depth, resulting in the need for additional investigations. Thermodynamic models (Tang et al., 2019; Ducea et al., 2021b) of arclogite partial melting yield primary magmas depleted in SiO_2 and enriched in alkalis, FeO, TiO_2, and Nb, but it is well known that at present, such models fail to reproduce the pressure-temperature-melt fraction relationships that control melt chemistry during partial melting (Lambart et al., 2016).

Based on the above geochemical fingerprints, albeit problematic, syn-drip arclogite-derived melts have been hypothesized to erupt along thickened continental arcs (Ducea et al., 2013; Murray et al., 2015; Kara et al., 2020) and within post-orogenic, rift-related alkaline-silicate complexes (Ducea et al., 2021b). However, in order to properly evaluate the importance of arclogite as a source of magmas in these settings, we must first better constrain the composition of arclogite-derived melts. To achieve this, we present in this paper the first partial melting experiments performed on an average amphibole-bearing arclogite composition at pressure and temperature conditions applicable to the sub-arc mantle, into which these rocks sink and pond.

2. Methods

2.1. Starting material

For our partial melting experiments, we use a synthetic hydrous arclogite composition (ARC15) consisting of reagent-grade oxides (SiO_2, TiO_2, FeO, MnO, MgO, P_2O_5), carbonates ($CaCO_3$, $NaCO_3$, K_2CO_3), and hydroxides ($Mg(OH)_2$). ARC15 was created to simulate a rock with a mineralogy composed of 15 wt.% amphibole (0.3 wt.% H_2O), 2 wt.% ilmenite, and equal proportions (41.5 wt.%) of garnet and clinopyroxene as well as a composition similar to that of average Sierran pyroxenite (Table 1, Fig. 1; Ducea, 2002). To synthesize this starting material, all oxides, excluding FeO, and carbonates were mixed under ethanol in an agate mortar for 60 min to ensure homogenization. Once dry, the material was poured into a Pt crucible and decarbonated inside a 1000 °C muffle furnace for ~10 h. To the mixture, we then introduced FeO and water (0.3 wt.%) as $Mg(OH)_2$. The material was then mixed in an agate mortar for 60 min. The starting powder, when not in use, was kept in a desiccator to prevent water absorption. Glass produced by a 1-hour super-liquidus piston cylinder experiment conducted at 1 GPa and 1600 °C was analyzed on the microprobe to determine the composition of the synthesized ARC15 starting material (Table 1). In major element

Table 2
Experimental run conditions and phase proportions (wt.%).

Run no.	T (°C)	P (GPa)	Duration (hours)	Melt	Cpx	Grt	Usp	Bi	Amp	Ilm	Fe loss (%)[1]	Σr^2[2]	fO_2 (ΔFMQ)[2]
98B	1040	2	92	–	49(2)	37(1)	–	1(1)	11(2)	2(0)	1.8	0.20	n.d.
75B	1080	2	211	+	55(2)	32(1)	2(0)	2(1)	10(3)	–	0.4	0.06	n.d.
83A	1100	2	138	+	54(2)	32(1)	2(0)	2(2)	9(4)	–	1.0	0.20	n.d.
74A	1140	2	68	+	65(1)	32(3)	2(0)	1(1)	–	–	0.4	0.10	n.d.
80B	1170	2	167	0(0)	61(1)	35(1)	2(0)	1(0)	–	–	0.2	0.24	−0.4(2)
72A	1190	2	68	5(2)	66(0)	27(2)	2(0)	–	–	–	0.8	0.16	−0.1(3)
67B	1220	2	62	7(1)	63(0)	27(1)	2(0)	–	–	–	1.1	0.15	−0.2(3)
77A	1240	2	68	13(1)	64(1)	21(1)	2(0)	–	–	–	1.8	0.27	−0.1(3)
78A	1270	2	68	15(3)	65(1)	19(1)	2(0)	–	–	–	1.1	0.12	−0.4(3)
70B	1300	2	95	18(2)	62(1)	17(1)	2(0)	–	–	–	1.6	0.29	−0.4(3)

Phase proportions for all runs are determined via mass balance on an anhydrous basis. 1σ errors are given in parentheses with least digits cited. Abbreviations are as follows: Cpx = clinopyroxene, Gt = garnet, Bi = biotite, Amph = amphibole, Usp = ulvöspinel, Ilm = ilmenite, – indicates phase is absent, + indicates melt is present as quenched crystals and did not yield robust chemical analyses, Σr^2 = sum of squared residuals, n.d. = not determined.

[1] Iron loss is calculated after mass balance according to the equation $100\ x\ (FeO_{starting\ composition} - FeO_{calculated})/FeO_{starting\ composition}$.

[2] fO_2 is calculated using Barr and Grove (2010) and reported as log units relative to the quartz-fayalite-magnetite (FMQ) buffer of O'Neill and Wall (1987) and Ballhaus et al. (1991).

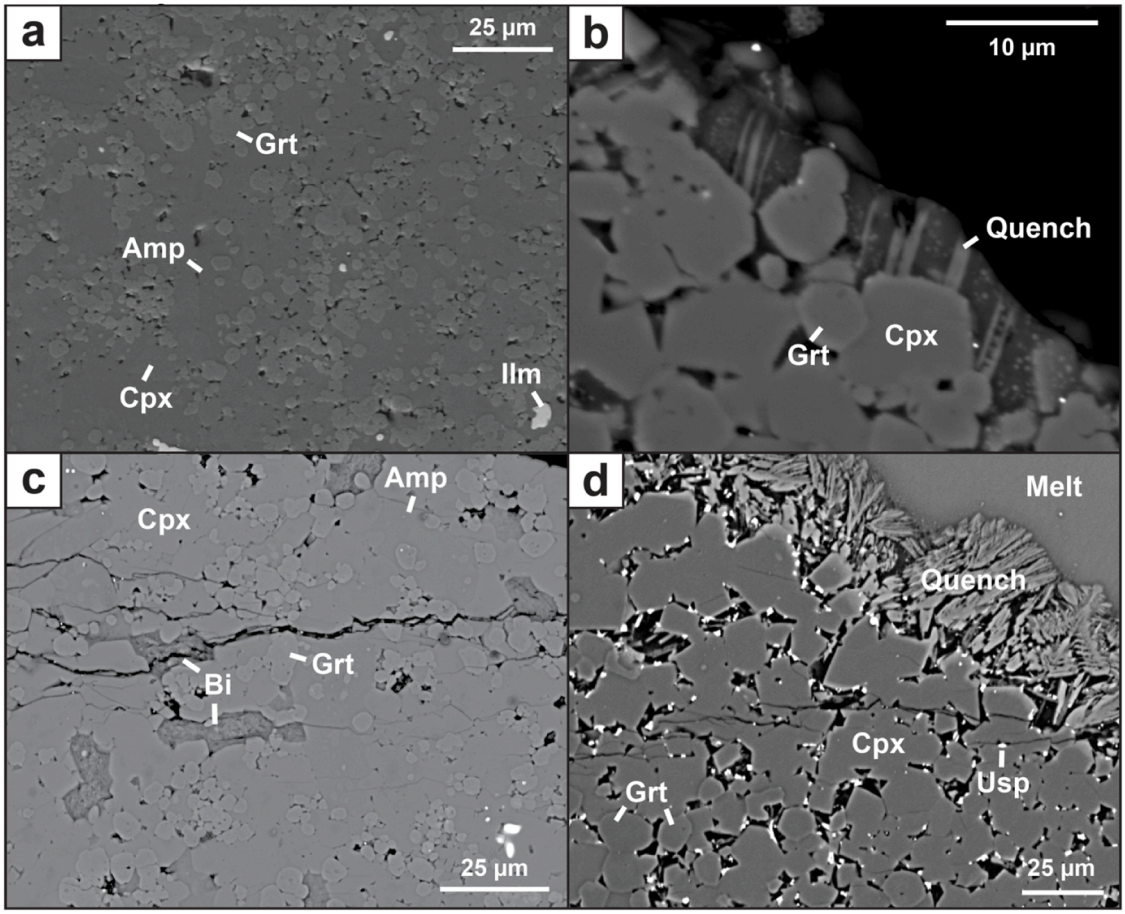

Fig. 2. Backscattered electron images of experiments at 2 GPa and 1040 °C (a), 1080 °C (b), 1100 °C (c), and 1220 °C (d). (a) Image from the inner capsule showing the subsolidus mineral assemblage, including clinopyroxene (Cpx), garnet (Grt), amphibole (Amp), and ilmenite (Ilm). (b) Image from the inner capsule showing the first appearance of melt in the form of quenched crystals coexisting with Cpx and Grt. (c) Image from the top of the inner capsule showing biotite (Bi) and Amp in equilibrium with Grt and Cpx. (d) Image from the top of the inner capsule showing Grt, Cpx, and ulvöspinel (Usp) separated from the melt pool by a region of quenched crystals. (For interpretation of the references to colour in this figure legend, the reader is referred to the web version of this article.)

space, ARC15 plots within the compositional range of natural arclogites (Fig. 1).

2.2. Experimental procedure

To minimize FeO and H_2O loss during experimental runs, the starting material was packed into HCl-cleaned $Au_{75}Pd_{25}$ double capsules (Kägi et al., 2005). The capsules were welded shut, situated between MgO spacers, and enclosed within a lead-lined $BaCO_3$ sleeve. Using a 150-ton end-loaded piston cylinder apparatus at the University of Arizona (UA), we conducted ten partial melting experiments from 1040 to 1300 °C. All experiments were performed at 2 GPa, a pressure that, depending on crustal thickness, could represent either the lower crust or the upper mantle beneath thick-crusted arcs. Following pressurization, the experimental charge was heated at 50 °C/min to achieve the desired temperature, which was regulated using a type-C thermocouple encased within an Al_2O_3 rod. Capsules were held at temperature for at least 62 h (Table 2), after which they were quenched, decompressed, mounted in epoxy, polished first with 400- to 800-grit silicon-carbide paper and then on velvet microcloth using 3- to 1 μm alumina paste, and finally carbon coated for textural and chemical analysis.

2.3. Analytical methods

Textural examination via back-scattered electron imaging and preliminary phase identification via energy-dispersive spectroscopy were first carried out for all experimental samples using the UA LaserChron Hitachi 3400 N scanning electron microscope. Individual phases in each sample were then analyzed for major element compositions using the CAMECA SX100 housed in the UA Lunar and Planetary Laboratory. All phase analyses were performed at 15 kV accelerating voltage with counting times of 20 s on peak and on background. A focused beam with a current of 20 nA was used for garnet, clinopyroxene, ulvöspinel, ilmenite, and amphibole analyses, while a defocused beam with a current of 10 nA and diameter of 2 μm and 10 μm was used for biotite and glass, respectively. To minimize its diffusion from the analysis site, sodium was measured first during all analyses. Phase compositions are reported in Supplementary Table S1. The presence of biotite was confirmed using a Renishaw InVia laser-Raman microscope at the UA Lunar and Planetary Laboratory (Supplementary Fig. S1).

3. Results

3.1. Approach to equilibrium

We argue that, despite the presence of some relict garnet cores, experiments operated under a closed system and achieved a close approach to thermodynamic equilibrium, based on: (1) The majority of crystalline phases and all pools of glass have geochemically homogenous compositions (Supplementary Table S1). Zoning was observed only in some garnet crystals, with care taken to avoid analyzing such grains. (2) Experiment durations (62–211 h) in this study are similar to or longer

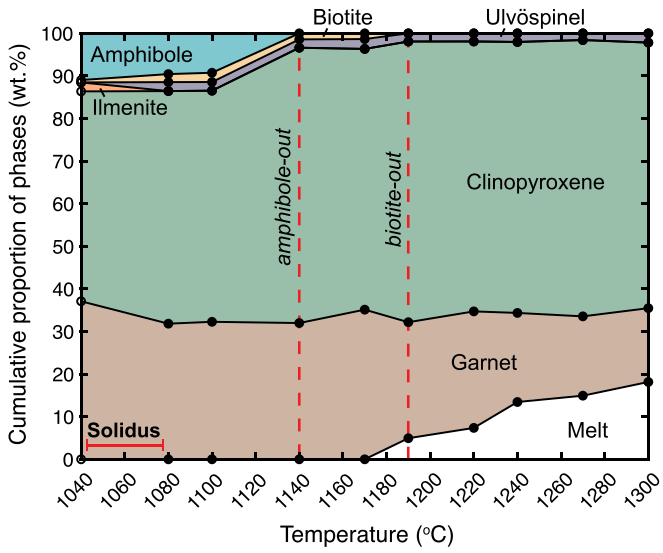

Fig. 3. Cumulative phase proportions (wt.%) in each experiment as a function of temperature (°C). Garnet is the main melt supplier during arclogite melting, as the modal abundance of garnet decreases with increasing proportion of melt. Open circles indicate sub-solidus experiments, whereas filled circles refer to experimental samples within which melt is present.

than published partial melting experiments that have demonstrated equilibrium on samples with compositions and volatile contents similar to ARC15 (Table 2; Médard et al., 2006; Sorbadere et al., 2013). (3) Low sums of squared residuals (0.06–0.29) and Fe losses (0.2–1.8%), both calculated from mass balance, indicate minimal alteration of the original bulk composition and maintenance of a closed system (Table 2). (4) K_D^{Fe-Mg} for clinopyroxene-melt and garnet-melt are, respectively, 0.35 ± 0.01 and 0.48 ± 0.04, values within error of those calculated for other high-pressure pyroxenite melting experiments (Keshav et al., 2004; Kogiso and Hirschmann, 2006; Lambart et al., 2013).

3.2. Oxygen fugacity

The oxygen fugacity relative to the fayalite-magnetite-quartz buffer (FMQ; O'Neill and Wall, 1987; Ballhaus et al., 1991) for melt-bearing charges was calculated according to the method of Barr and Grove (2010), which uses as inputs the Fe contents of the melt and the Au-Pd capsule adjacent to the melt pool. In experimental samples, fO_2 ranges between ΔFMQ −0.4 ± 0.3 to −0.2 ± 0.3 (Table 2), within error of the fO_2 estimated for the primitive magma (ΔFMQ −1.0 ± 1.0) in equilibrium with arclogitic cumulates from the Colorado Plateau (Tang et al., 2018).

3.3. Phase assemblages and melting reactions

Experimental conditions and phase proportions are reported in Table 2. Modal proportions were determined using mass balance, with errors on phase proportions calculated by propagation of standard deviations on oxide contents. All experimental charges (Fig. 2, Supplementary Fig. S2) are composed primarily of augitic clinopyroxene (49–66 wt.%), which coexists throughout the studied temperature range with lesser amounts of garnet (17–37 wt.%). An Fe-Ti oxide phase (2 wt.%) also exists in all experimental samples in the form of ilmenite at subsolidus temperatures and ulvöspinel at suprasolidus temperatures. Finally, pargasitic amphibole (9–11 wt.%) and minor biotite (1–2 wt.%) are present in the lowest temperature runs.

Prior to partial melting (run 98B, 1040 °C), ARC15 comprises clinopyroxene (49 wt.%), garnet (37 wt.%), amphibole (11 wt.%), ilmenite (2 wt.%), and biotite (1 wt.%; Figs. 2 and 3). The first melt appears in the form of quenched crystals at 1080 °C, placing the hydrous arclogite solidus between 1040 and 1080 °C. Near-solidus partial melting is controlled by amphibole dehydration, as the first addition of melt coincides with a decrease in amphibole mode as well as a transition in oxide phase from ilmenite to ulvöspinel (Fig. 3) following the reaction:

Garnet + Amphibole + Ilmenite = Clinopyroxene + Ulvöspinel + Melt. (1)

After the ilmenite-ulvöspinel transition, partial melting continues via the dehydration of amphibole, which disappears fully by 1140 °C to form clinopyroxene and melt according to the reaction:

Amphibole = Clinopyroxene + Melt. (2)

Following amphibole-out, between 1140 and 1190 °C, clinopyroxene and melt are produced at the expense of garnet and biotite following the reaction:

Garnet + Biotite = Clinopyroxene + Melt. (3)

Reactions (1), (2), and (3) could not be defined quantitatively owing to the lack of quantifiable melt fractions in near-solidus experiments. Rather, these reactions were estimated based on changes in the proportions of experimental phases with increasing temperature (Supplementary Fig. S3a-c). Once biotite is exhausted at 1190 °C, the melting reaction shifts to:

0.8 Garnet + 0.2 Clinopyroxene = 1 Melt, (4)

such that garnet is preferentially consumed over clinopyroxene and is thus the main supplier of melt. Coefficients for reaction (4) were estimated via least-squares weighted regression (Supplementary Fig. S3d) according to the method of Baker and Stolper (1994) and normalized to 1 g of melt. Reaction (4) and its coefficients resemble those determined for other silica-deficient pyroxenites at 2 GPa (e.g., Lambart et al., 2013). If reaction (4) remains valid with increasing temperature, it can be assumed that a garnet-free clinopyroxenitic residue will form as the liquidus is approached.

3.4. Melt and mineral compositions

Phase compositions for each experimental run are listed in Supplementary Table S1. Melts derived from ARC15 are characterized by high TiO_2 (2.54–3.73 wt.%), FeO (9.83–17.01 wt.%), Na_2O (2.13–2.94 wt.%), and K_2O (0.96–3.74 wt.%) contents and low SiO_2 (43.36–51.86 wt.%) and MgO (4.61–8.78 wt.%) contents. With rising melt fractions, SiO_2, K_2O, and Al_2O_3 (13.77–16.56 wt.%) concentrations in the melt systematically decrease, while MgO, FeO, and CaO (6.85–10.09 wt.%) contents increase (Fig. 4). Both TiO_2 and Na_2O initially increase with melt fraction, but experience decreases with further melting. Overall, arclogite melts vary in composition from low-F basaltic trachy-andesite at near-solidus temperatures (1170 °C), to trachy-basalt at higher temperatures (1190 °C) and melt fractions (5 wt.%), and to high-F (7–18 wt.%) basanite at the highest temperatures investigated (1220–1300 °C; Fig. 5a).

All experiments contain augite, which has relatively high Na_2O (1.05–1.74 wt.%) and Al_2O_3 (4.82–9.20 wt.%) contents (Supplementary Table S1). While the Al_2O_3 content of clinopyroxene increases with temperature, Na_2O decreases. Likewise, as temperatures rise, the CaO (16.71–19.62 wt.%) content of clinopyroxene decreases, with sharp drops corresponding to amphibole- and biotite-out. For the three main suprasolidus phases, the MgO contents largely increase with higher temperature runs: clinopyroxene MgO generally increases from 13.11 to 14.21 wt.%, ulvöspinel MgO rises from 2.95 to 4.24 wt.%, and garnet becomes increasingly pyrope-rich as MgO (12.43–15.97 wt.%) increases and FeO (13.69–17.18 wt.%) decreases, a trend that is observed in other pyroxenite experiments (e.g., Borghini and Fumagalli, 2020). Biotite, while present, displays subtle increases in TiO_2 (4.16–5.01 wt.%) and

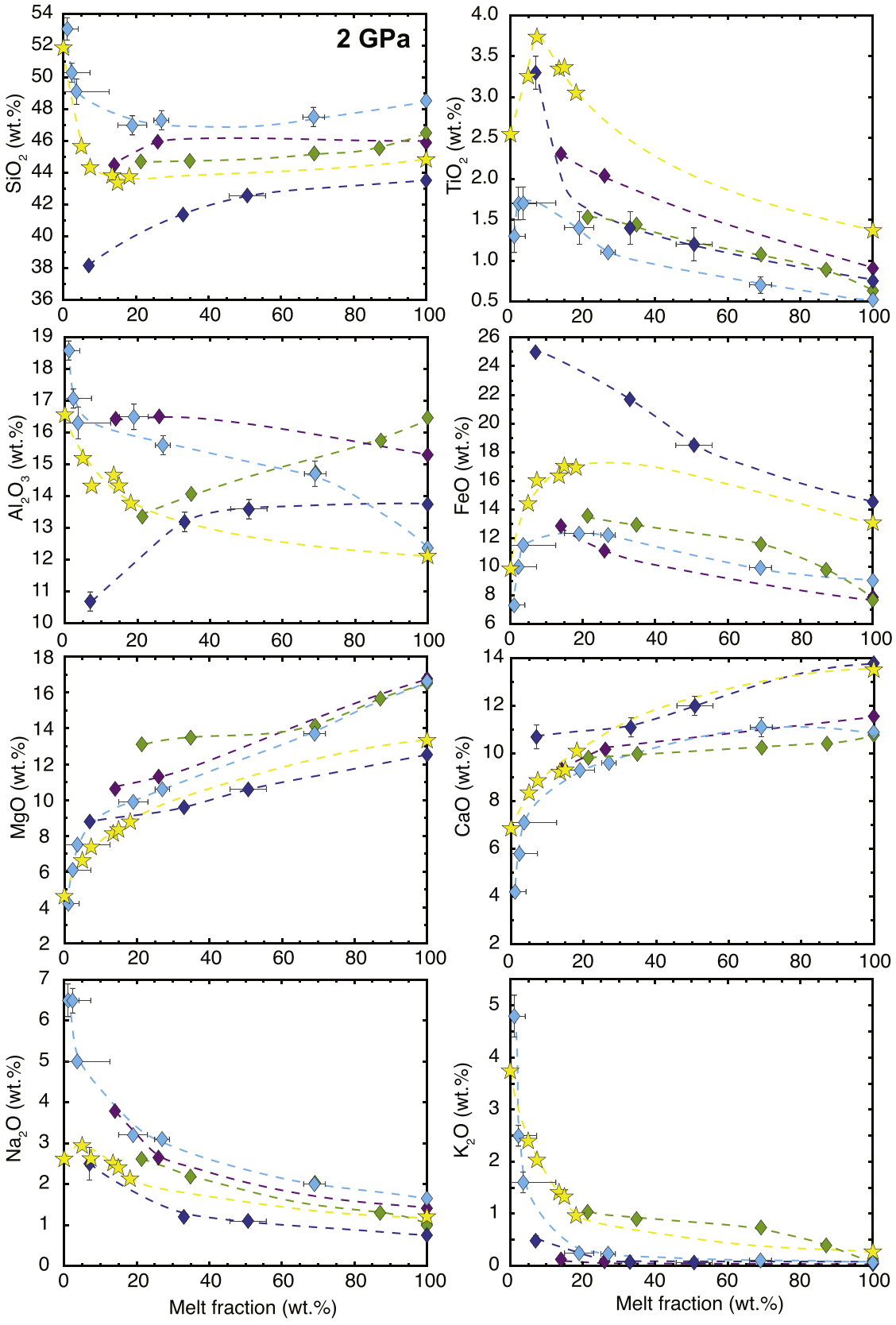

Fig. 4. Major element oxide contents of arclogite melts versus melt fraction (wt.%). Also shown are melt compositions from anhydrous silica-deficient (SD) pyroxenite melting experiments conducted at 2 GPa. Error bars on melt fractions and oxide contents are shown for this study and for previously published data when reported in the original paper (Hirschmann et al., 2003; Keshav et al., 2004; Lambart et al., 2013). When not visible, error bars are included within the symbol. Legend as in Fig. 1.

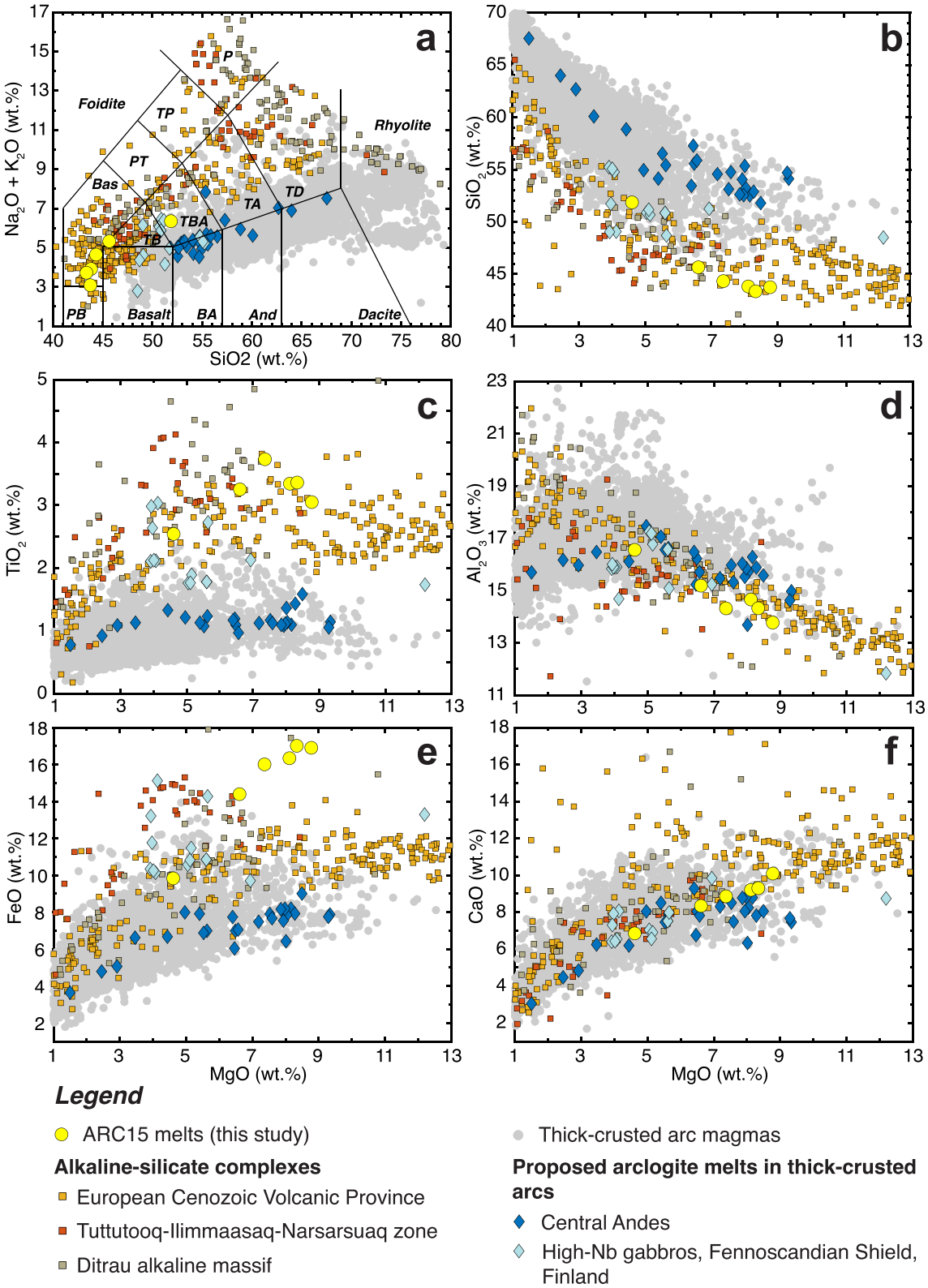

Fig. 5. Total alkali-silica diagram (a) and major element oxide-MgO diagrams (b-f) of experimental ARC15 melts compared to arc volcanics emplaced upon >40 km-thick crust (Aleutian arc, Andean arc, Cascade arc, Central American volcanic arc, Honshu arc, Izu-Bonin arc, Kamchatka arc, Kurile arc, Mexican Volcanic Belt, Sunda arc, New Zealand arc), magmas from the central Andes (Ducea et al., 2013; Murray et al., 2015) and Fennoscandian Shield (Kara et al., 2020) previously interpreted to be derived from arclogites, and magmas from alkaline-silicate complexes. ARC15 melts plot outside of the compositional field of thick-crusted arc magmas but overlap with alkaline-silicate complexes. Arclogite melting is therefore not a dominant source of magmatism at thick-crusted arcs but may contribute significantly to the formation of alkaline-silicate complexes. Abbreviations in (a) are as follows: PB = picro-basalt, BA = basaltic andesite, And = andesite, TB = trachy-basalt, BTA = basaltic trachy-andesite, TA = trachyandesite, TD = trachydacite, Bas = basanite, PT = phono-tephrite, TP = tephri-phonolite. (For interpretation of the references to colour in this figure legend, the reader is referred to the web version of this article.)

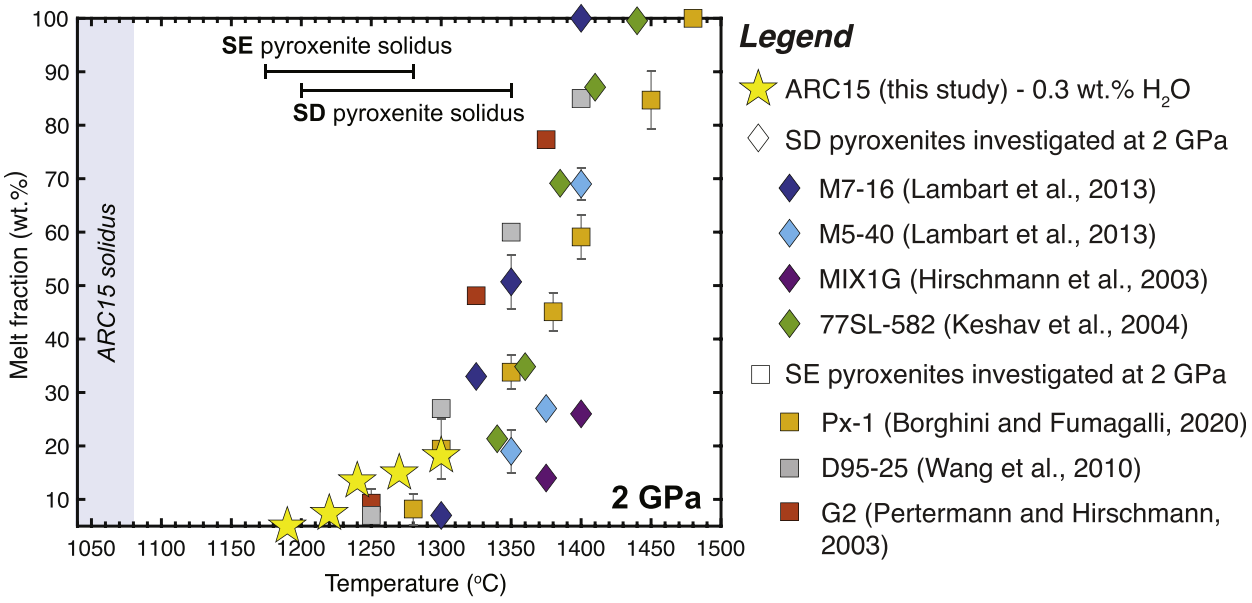

Fig. 6. Melt fraction (wt.%) vs. temperature (°C) for ARC15 compared to dry silica-deficient (SD) and silica-excess (SE) pyroxenites investigated at 2 GPa. Reported solidi ranges for ARC15 (1040–1080 °C), SD pyroxenites (1200–1350 °C), and SE pyroxenites (1175–1280 °C) are highlighted. Error bars on melt fractions are shown for this study and for previously published data when reported in the original paper (Pertermann and Hirschmann, 2003; Lambart et al., 2013; Borghini and Fumagalli, 2020). When not visible, error bars are included within the symbol. (For interpretation of the references to colour in this figure legend, the reader is referred to the web version of this article.)

FeO (11.64–12.88 wt.%) and decreases in MgO (15.97–17.48 wt.%) and SiO_2 (38.67–39.83 wt.%) with temperature. Amphibole, stable only in the three lowest temperature (1040, 1080, and 1100 °C) experiments, displays an enrichment in FeO (11.11–12.02 wt.%) compared to experimental (Sorbadere et al., 2013) and natural (Lee et al., 2006) cumulate-hosted pargasite.

4. Discussion

4.1. Solidus temperature and melt productivity

Our results bracket the dehydration solidus of arclogite between 1040 and 1080 °C, which, owing to the addition of water (0.3 wt.%), is 120–310 °C lower than the solidi (1200–1350 °C) determined for other nominally anhydrous SD garnet pyroxenite compositions at 2 GPa (Fig. 6; Hirschmann et al., 2003; Keshav et al., 2004; Lambart et al., 2013). In fact, since hydrous arclogite begins melting at temperatures lower than the solidus range of more fertile SE garnet pyroxenites (1175–1280 °C; Pertermann and Hirschmann, 2003; Wang et al., 2010; Borghini and Fumagalli, 2020), the effect of small amounts of volatiles in depressing the solidus seems to overcome the opposing effect of chemical depletion.

At melt fractions (F) > 5 wt.%, the amount of melt produced during partial melting of ARC15 increases linearly with temperature, as is roughly observed for other experimental pyroxenites (Fig. 6). Using only experiments with ≥ 5 wt.% melt, we approximate an isobaric melt productivity for each composition as the linear change in F from the lowest (T_i) to the highest (T_f) experimental temperature $[(\Delta F/\Delta T)_P = (F_{Tf} - F_{Ti})/(T_f - T_i)]$. ARC15 has a $(\Delta F/\Delta T)_P$ of 0.12%/°C, whereas both anhydrous SD and SE pyroxenites display much higher melt productivities (0.46–0.93%/°C). Therefore, although ARC15 begins melting earlier than any anhydrous experimental pyroxenitic composition, this composition is the least melt-productive of all experimental pyroxenites for melt fractions between 5 and 20 wt.%. This depression in both the solidus temperature and melt productivity of hydrous arclogite versus anhydrous pyroxenite, also displayed during the partial melting of hydrous peridotites compared to their anhydrous counterparts, has been attributed to the involvement of water (Gaetani and Grove, 1998).

4.2. Geochemistry of arclogite-derived magmas and comparison to other experimental pyroxenite melts

During partial melting, significant changes in the major element composition of ARC15-derived melts reflect the partitioning behavior of these elements between the melt and the solid residue (Fig. 4). As ARC15 melts, the FeO, MgO, and CaO contents of the melt increase, signifying the compatible nature of these elements in the clinopyroxene- and garnet-rich residue (Supplementary Fig. S4). Contrasting behavior is exhibited by SiO_2, Al_2O_3, and K_2O, all of which are enriched in near-solidus melts and decrease significantly with increasing melt fraction. While K_2O acts incompatibly in the majority of the residual mineralogy, the incompatibility of SiO_2 and Al_2O_3 in the bulk residue at low melt fractions is primarily controlled by the incompatible nature of these oxides in residual garnet and clinopyroxene, respectively. Finally, both the Na_2O and TiO_2 contents of the melt initially increase at low F and then decrease with further melting, the kink in these curves corresponding to decreases in the compatibility of Na_2O in clinopyroxene and TiO_2 in ulvöspinel, respectively (Supplementary Fig. S4).

As a result, in part, of these trends, melts sourced from ARC15 have major element compositions mostly within the range of other SD pyroxenite-derived melts (Fig. 4). Specifically, hydrous arclogite, like other SD pyroxenites, yields SiO_2-poor and alkali-rich melts. In contrast to other SD pyroxenites, however, experimental arclogite-derived glasses have anomalously high TiO_2 and FeO contents, likely due to the inherent enrichment in these oxides of ARC15. Furthermore, ARC15 melts, with low MgO contents (4.61–8.78 wt.%) and Mg#s (0.45–0.48), are generally less primitive compared to other SD pyroxenites, which at similar melt fractions have MgO contents between 4 and 13 wt.% and Mg#s between 0.39–0.63. It is interesting to note that, as a result of their MgO-poor and FeO-rich nature, parental arclogite melts derived from ARC15-like compositions are commonly excluded from compilations of primitive arc basalts (e.g., Schmidt and Jagoutz, 2017), which use MgO or Mg# cutoffs to remove seemingly evolved samples. Parental magmas sourced from SE pyroxenites are also eliminated from these

compilations, as they have MgO contents typically less than 8 wt.% (Lambart et al., 2013). We therefore caution against using such arbitrary geochemical filters in petrogenetic studies, especially since non-peridotitic lithologies have been recognized to contribute to magmatism in most tectonomagmatic settings (Mallik et al., 2021).

4.3. Comparison to natural magmas

Using our experimental results, we can now investigate whether arclogite melting is a significant magma-generating process in 1) thick-crusted arcs and 2) post-orogenic alkaline-silicate complexes.

4.3.1. Arclogite contribution to thick-crusted arc magmatism

Arclogites form as products of differentiation and/or partial melting in the lower crust of thick-crusted (>40 km) arcs (Ducea et al., 2021a), where the Moho extends to pressures great enough to stabilize garnet in basaltic compositions (>1.2 GPa; Blatter et al., 2023). Temperatures in the subarc lower crust have been constrained by thermometry (Lee et al., 2006; Depine et al., 2008; Zieman et al., 2023) and numerical modeling (Annen et al., 2006; Jackson et al., 2018) to be between 700 and 1200 °C, too cold to melt hydrous arclogites in substantive amounts as determined by our experiments. Rather, because the mantle wedge can at 3 GPa reach temperatures of >1400 °C (Syracuse et al., 2010), arclogites likely experience extensive partial melting as they founder into the subarc mantle (Elkins-Tanton, 2007). It is then plausible that arclogites may be an important source of arc magmatism. To evaluate this possibility, we compiled geochemical data for Pliocene-Holocene volcanics from arcs with modern crustal thicknesses greater than 40 km using the GEOROC database (https://georoc.eu/). Data filtering methods, crustal thickness calculations, and the final compilation are included in the Supplementary Materials.

Fig. 5 compares the major element compositions of thick-crusted arc magmas with those of our experimental arclogite melts. Typical thick-crusted arc magmas are far too SiO_2-rich and alkali-, FeO-, and TiO_2-poor to represent primary arclogite melts or to be derived predominantly from arclogite. Samples from the central Andean Altiplano-Puna plateau previously proposed to be arclogite-derived on the basis of Zn/Fe ratios (Ducea et al., 2013; Murray et al., 2015) do not actually display major element compositions consistent with this interpretation, and are more likely derived from pyroxenite veins in the subarc mantle (Bowman and Ducea, 2023). Based on major element comparisons, we argue that arclogite melting is not a dominant mechanism of magmagenesis in thick-crusted arc settings. We recognize that this conclusion is highly dependent upon the composition of the experimental starting material and the pressure at which it is investigated. For example, compositions on the extreme FeO-poor and SiO_2- and MgO-rich end of the arclogite compositional spectrum (Fig. 1), such as M5–40 (Lambart et al., 2013), may produce melts with major element geochemical signatures more similar to those of thick-crusted arc magmas; however, the majority of arclogites are too SiO_2-poor and FeO-rich (Fig. 1) to generate melts that geochemically resemble thick-crusted arc magmas. In addition, partial melting of ARC15 at higher pressures would increase the stability of garnet in the residue (Kogiso et al., 2003), allowing clinopyroxene, a comparatively SiO_2-rich phase, to contribute increasingly to melting and potentially bringing arclogite-derived melts into the compositional field of thick-crusted arc magmatism. Additional experiments on arclogite compositions at higher pressures are therefore necessary to constrain the effect of pressure on melt geochemistry.

Overall, our data suggest an apparent absence of primary arclogite-derived magmas at thick-crusted arcs, which may be due in part to the transient nature of the arclogitic source: foundering arclogite bodies may only reside in the subarc melting region during finite periods of time that mirror the tempo of orogenic cyclicity. Yet the temperature regime of the subarc mantle (>1200 °C; Kelemen et al., 2004; Syracuse et al., 2010) exceeds the solidus of hydrous arclogite (1040–1080 °C), especially if hot mantle upwells in response to dripping, so why do primary arclogite-derived melts seem to be missing from the magmatic record at thick-crusted arcs? It is possible that, due to the shape of isotherms in the mantle wedge of subduction zones, arclogites that sink rapidly through the hot core of the mantle wedge may avoid conductive heating in excess of their solidus temperature and escape partial melting; however, such rapid descent requires large-sized and low-viscosity arclogitic material that may not be representative for all arcs (Elkins-Tanton, 2007). It is therefore more likely that arclogite-derived melts in the subarc region, whether formed in the mantle or in the lower crust, are modified by secondary processes that completely mask their characteristic major element signatures. For instance, arclogite melts are not in equilibrium with peridotite and are likely to react as they ascend through the mantle (Lambart et al., 2012). Melt-rock reaction, however, should not substantially decrease the originally high TiO_2 content of the arclogite-derived melt. We therefore do not favor a primary role of arclogite melt-peridotite reaction in generating thick-crusted arc magmas. In addition, since arclogites have low melt productivities, their melts may be of sufficiently low melt fraction that they are diluted by more voluminous magmas sourced from i.e., wedge peridotite (Grove et al., 2012), pyroxenites from the downgoing oceanic crust (Schmidt and Jagoutz, 2017) or subarc mantle (Bowman and Ducea, 2023), and assimilated continental lower crust (Ducea and Barton, 2007). This is interpreted to be the case for the Taapaca dacite dome complex in the central Andes, where arclogite has been identified via polytopic vector analysis as one of three end-member compositions involved in the petrogenesis of these volcanics (Blum-Oeste and Wörner, 2016).

According to Fig. 5, only the high-Nb gabbros emplaced in the Fennoscandian Shield, Finland during the thick-crusted Paleoproterozoic Svecofennian orogen show major element signatures indicative of an arclogite origin (Kara et al., 2020). Interestingly, these gabbros intruded during an intra-orogenic extensional phase that resulted in the development of multiple rift basins (Bergman et al., 2008). Perhaps, in contrast to orogenic contractional regimes that restrict the eruption of primary magmas along thickened arcs (Loucks, 2021), continental extension provides pathways for arclogite-derived magmas to ascend rapidly and avoid alteration. Such is the case along the East African rift system, where melting of pyroxenitic drips has been interpreted to occur (Furman et al., 2016).

4.3.2. Arclogite contribution to alkaline-silicate complexes

Because continental rifting follows orogenesis, a sequence that forms the foundation of the Wilson Cycle (Wilson et al., 2019), arclogites that formed and foundered during subduction beneath thick-crusted arcs inevitably comprise a portion of the asthenospheric mantle that upwells and melts beneath the subsequently collapsing orogen. As a result, arclogite melts may more recognizably manifest on the surface of the Earth during periods of orogenic collapse and post-orogenic rifting, as extensional stresses associated with these events promote the eruption of primitive magmas (Loucks, 2021). Arclogite melts generated during such post-orogenic rifting also likely experience limited melt-peridotite reaction as they ascend mantle that has already undergone previous metasomatism by syn-subduction arclogite-derived magmas, thus contributing to the preservation of their diagnostic geochemical signatures. In fact, arclogite-derived melts have been shown via thermodynamic modeling to geochemically resemble magmas erupted at alkaline-silicate complexes (Ducea et al., 2021b), which form in post-orogenic extensional regimes (Goodenough et al., 2021; Beard et al., 2023). Such complexes host massifs of alkali-rich, feldspathoid-bearing igneous rocks and are important sources of rare-earth elements (REE), particularly the heavy REE (HREE; Goodenough et al., 2016; Beard et al., 2023). The current consensus is that these anomalous magmatic systems derive from low-degree partial melting of metasomatized and heterogeneous subcontinental lithospheric mantle (Smith et al., 2016; Marks and Markl, 2017; Braunger et al., 2020; Goodenough et al., 2021; Beard et al., 2023). Yet vital components of this model, such

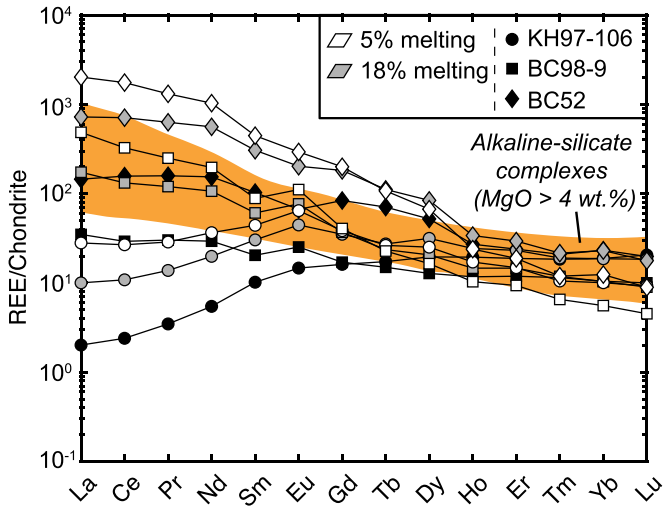

Fig. 7. Chondrite-normalized (McDonough and Sun, 1995) rare-earth element patterns for natural arclogite samples KH97–106 (depleted end-member; Dhuime et al., 2007), BC98–9 (intermediate composition; Lee et al., 2006) and BC52 (enriched end-member; Lee et al., 2006). Assuming non-modal batch melting, we also plot predicted rare-earth element patterns of melts derived from these three compositions for 5% and 18% partial melting. (For interpretation of the references to colour in this figure legend, the reader is referred to the web version of this article.)

as the composition of the lithospheric mantle, the metasomatic agent, and the conditions necessary to bring about low-degree melting in regions of rifting and hot mantle upwelling, remain vague. Partial melting of arclogites, which are inherently silica-poor and melt-depleted, presents an alternative model for the formation of these complexes (Ducea et al., 2021b). To test this hypothesis, we compare the geochemistry of our experimental melts to three extension-related alkaline-silicate provinces that do not require the involvement of mantle plumes in their petrogenesis: 1) Tuttutooq-Ilimmaasaq-Narsarsuaq (TIN) zone, Greenland (Hutchison et al., 2021), 2) European Cenozoic Volcanic Province (Binder et al., 2024), and 3) Ditrau Alkaline Massif, Romania (Pál-Molnár et al., 2015). Each of these provinces hosts significant enrichments in the REEs (Goodenough et al., 2016; Beard et al., 2023) – the TIN and Ditrau provinces to an economic degree – and are spatially associated with and postdate major orogenic events (Pál-Molnár et al., 2015; Hutchison et al., 2021; Binder et al., 2024). The TIN zone in the Gardar rift, for example, is interpreted to tap mantle metasomatized 500 My earlier by Andean-type subduction during the thickened Ketilidian orogen (Hutchison et al., 2021). Likewise, the European Cenozoic Volcanic Province, which was emplaced on top of Variscan basement, hosts magmas interpreted to derive from lithospheric mantle enriched via subduction-metasomatism during the ~300 Ma Variscan orogeny (e.g., Binder et al., 2024).

As shown in Fig. 5, there is remarkable overlap in the major element compositions of arclogite melts and alkaline-silicate complexes. In particular, arclogite-derived magmas reproduce the anomalously low SiO_2 and high TiO_2 and alkali contents that characterize these complexes. Only the FeO and MgO concentrations of the two magmatic suites disagree: alkaline-silicate complexes display higher MgO and lower FeO compared to arclogite melts. Perhaps these alkaline magmas originated from arclogites with higher MgO and lower FeO contents compared to our starting material, a likely scenario given the geochemical variability of natural arclogites (Fig. 1). It is also plausible that as evolved (Mg# = 0.45–0.48), silica-undersaturated, FeO-rich arclogite melts ascend through the mantle, these melts react with ambient high-Mg# olivine, resulting in Fe-Mg melt/rock exchange that decreases the FeO content and increases the MgO content of the reacting arclogite-derived melt (Ackerman et al., 2009).

To further assess the possible genetic relationship between arclogite melts and alkaline-silicate complexes, it is necessary to relate their trace element signatures. To do this, we use non-modal batch melting to model the trace element compositions of arclogite melts after 5 and 18% melting. We limit our analysis to the REEs, as arclogites have far too variable large ion lithophile and high field strength element concentrations to produce meaningful results. Our models use three different starting arclogite compositions: 1) KH97–106 (Dhuime et al., 2007) from the Kohistan arc crustal section, a depleted arclogite endmember representing unaltered lower crustal cumulate material that has somehow escaped foundering, 2) BC52 (Lee et al., 2006) from the Sierra Nevada xenolith suite, an enriched arclogite endmember, and 3) BC98–9 (Lee et al., 2006) also from the Sierra Nevada, which has a composition between the two extremes. The latter two samples from the Sierra Nevada (BC52 and BC98–9) represent foundered residues that have experienced some degree of metasomatic LREE enrichment (Lee et al., 2006), a process likely to occur as arclogites sink through subduction-influenced mantle. We note that we do not consider the role

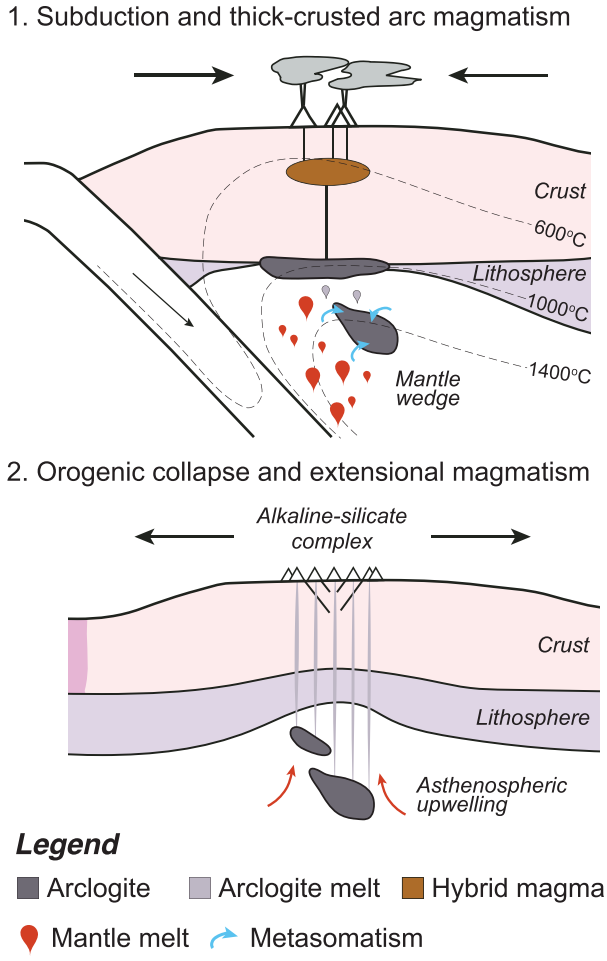

Fig. 8. Schematic depicting (1) arclogite formation, foundering, metasomatism, and partial melting at thick-crusted arcs. Rather than erupting on the surface of the Earth as primitive melts, arclogite-derived magmas are modified by secondary processes, such as magma mixing, to produce hybrid magma typical of thick-crusted arcs. Isotherms after Holwell et al. (2022). (2) Post-subduction orogenic collapse and lithospheric extension incite asthenospheric upwelling and partial melting of foundered, metasomatized arclogite. Extension and previous subduction-related mantle metasomatism promote the transport of primitive arclogite melts to the surface to form alkaline-silicate complexes. (For interpretation of the references to colour in this figure legend, the reader is referred to the web version of this article.)

of peridotite melting in our models, as the temperature range of investigation (1190–1300 °C) is below the peridotite solidus at 2 GPa (~1350; Hirschmann et al., 2000). Since ARC15 has a lower solidus temperature than peridotite, rather than mixing with peridotite-derived melts, arclogite melts likely react with subsolidus peridotite as they ascend the mantle.

Results of our arclogite batch melting models, which use the phase assemblages (excluding ulvöspinel) and reactions determined in this study as well as partition coefficients from Green et al. (2000), Pertermann et al. (2004), and Adam and Green (2006), are shown in Fig. 7. The range of REE patterns for the three alkaline-silicate complexes, now filtered to include only samples with MgO contents greater than 4 wt.%, are shown in orange. It is clear that the HREE contents of arclogite melts and alkaline-silicate magmas perfectly correlate, a significant finding as alkaline-silicate complexes are valuable hosts of the most societally critical HREEs (Wall, 2014). This correlation points to arclogites as a potential initial source of HREEs in these complexes, which is plausible since garnet, an HREE repository, is the main melt contributor during arclogite melting. Still, secondary processes, such as fractional crystallization and shallow fluid-mediated processes, are required to elevate magmatic REE contents to economically viable concentrations (Chakhmouradian and Zaitsev, 2012). Moreover, our models show that the depleted and enriched arclogite endmembers produce melts that neatly bracket the LREE contents of magmas from alkaline-silicate systems, while melts of the intermediately enriched arclogite composition plot directly in the field of these alkaline magmas. Hence, partial melting of arclogites that have experienced metasomatism and associated LREE enrichment during their residence in the subduction-influenced mantle may be fundamental in generating magmas that form post-orogenic alkaline-silicate complexes and associated REE deposits.

5. Geodynamic setting of arclogite melting and concluding remarks

We demonstrate that at 2 GPa, amphibole-bearing arclogites, prevalent at the base of thick-crusted arcs as density-unstable residues, begin melting between 1040 and 1080 °C either in-situ in the lower crust or as they founder into the sub-arc mantle. Arclogites have the lowest melt productivities of experimentally investigated pyroxenites and produce melts that are silica-undersaturated, alkalic, and rich in TiO_2 and FeO. Based on major element geochemistry, arclogite melts cannot be significant contributors to thick-crusted arc magmatism. Rather, the major and trace element geochemical signatures of melts derived from mildly enriched arclogites match those of alkaline-silicate complexes, which erupt during post-orogenic extensional events and are famous for their well-endowed REE deposits (Goodenough et al., 2021; Beard et al., 2023). Our results are consistent with a conceptual model (Fig. 8a) in which arclogites form along thickened arcs and experience variable degrees of metasomatism and LREE enrichment as they detach from the lower crust and sink through the subduction-influenced mantle. During this stage, melts derived from arclogitic residues likely react with ambient mantle peridotite as they migrate upward, thus creating pathways for later arclogite-derived melts to ascend the mantle with minimal reaction. Once they reach the crust, these melts are likely modified by further syn-subduction secondary processes, such as magma mixing, that obscure their characteristic geochemical signals. As subduction wanes and orogenic collapse ensues (Fig. 8b), continental extension drives asthenospheric upwelling and melting of the arclogite-bearing mantle. Arclogite-derived melts during this stage experience only minor melt-peridotite reaction as they move through the previously metasomatized mantle. Extensional stresses facilitate the ascent of primitive arclogite-derived magmas through the lithosphere (Loucks, 2021), contributing to the formation of alkaline-silicate complexes and, potentially, their associated REE deposits.

CRediT authorship contribution statement

Emilie E. Bowman: Conceptualization, Data curation, Formal analysis, Investigation, Writing – original draft, Writing – review & editing. **Ananya Mallik:** Writing – review & editing, Resources, Methodology, Funding acquisition, Conceptualization. **Mihai N. Ducea:** Funding acquisition, Conceptualization, Writing – review & editing.

Declaration of competing interest

The authors declare that they have no known competing financial interests or personal relationships that could have appeared to influence the work reported in this paper.

Data availability

All data used in this manuscript is available online in the Supplementary Material.

Acknowledgements

A.M. acknowledges support from National Science Foundation grant EAR2138410. M.N.D. acknowledges support from National Science Foundation grant EAR2020935 and funding by the program (PNRR-III-C9-2023–I8) of Romanian MCID (64/30.07.2023). We acknowledge NASA grants #NNX12AL47G and #NNX15AJ22G and NSF grant #1531243 for funding of the instrumentation in the Kuiper Materials Imaging and Characterization Facility at the University of Arizona. We thank Ken Domanik, Zachary Michels, and Zoe Zeszut for assistance on the microprobe, SEM, and Raman, respectively. Early discussions with Antoine Triantafyllou greatly benefited the paper. We thank Rosemary Hickey-Vargas for editorial handling. Constructive reviews by Veronique Le Roux and Etienne Médard greatly improved the paper.

Supplementary materials

Supplementary material associated with this article can be found, in the online version, at doi:10.1016/j.epsl.2024.118952.

References

Ackerman, L., Jelínek, E., Medaris, G., Ježek, J., Siebel, W., Strnad, L., 2009. Geochemistry of Fe-rich peridotites and associated pyroxenites from Horní Bory, Bohemian Massif: insights into subduction-related melt–rock reactions. Chem. Geol. 259, 152–167. https://doi.org/10.1016/j.chemgeo.2008.10.042.

Adam, J., Green, T., 2006. Trace element partitioning between mica- and amphibole-bearing garnet lherzolite and hydrous basanitic melt: 1. Experimental results and the investigation of controls on partitioning behaviour. Contrib. Mineral. Petrol. 152, 1–17. https://doi.org/10.1007/s00410-006-0085-4.

Annen, C., Blundy, J.D., Sparks, R.S.J., 2006. The genesis of intermediate and silicic magmas in deep crustal hot zones. J. Petrol. 47, 505–539. https://doi.org/10.1093/petrology/egi084.

Baker, M.B., Stolper, E.M., 1994. Determining the composition of high-pressure mantle melts using diamond aggregates. Geochim. Cosmochim. Acta 58, 2811–2827. https://doi.org/10.1016/0016-7037(94)90116-3.

Ballhaus, C., Berry, R.F., Green, D.H., 1991. High pressure experimental calibration of the olivine-orthopyroxene-spinel oxygen geobarometer: implications for the oxidation state of the upper mantle. Contrib. Mineral. Petrol. 107, 27–40. https://doi.org/10.1007/BF00311183.

Barr, J.A., Grove, T.L., 2010. AuPdFe ternary solution model and applications to understanding the fO2 of hydrous, high-pressure experiments. Contrib. Mineral. Petrol. 160, 631–643. https://doi.org/10.1007/s00410-010-0497-z.

Beard, C.D., Goodenough, K.M., Borst, A.M., Wall, F., Siegfried, P.R., Deady, E.A., Pohl, C., Hutchison, W., Finch, A.A., Walter, B.F., Elliott, H.A.L., Brauch, K., 2023. Alkaline-Silicate REE-HFSE Systems. Econ. Geol. 118, 177–208. https://doi.org/10.5382/econgeo.4956.

Bergman, S., Högdahl, K., Nironen, M., Ogenhall, E., Sjöström, H., Lundqvist, L., Lahtinen, R., 2008. Timing of Palaeoproterozoic intra-orogenic sedimentation in the central Fennoscandian Shield; evidence from detrital zircon in metasandstone. Precambrian. Res. 161, 231–249. https://doi.org/10.1016/j.precamres.2007.08.007.

Binder, T., Marks, M.A.W., Walter, B.F., Wenzel, T., Markl, G., 2024. Two distinct metasomatized mantle sources produced two groups of alkaline SiO2-undersaturated rocks in the Southern Central European volcanic province. J. Petrol. 65, egae070. https://doi.org/10.1093/petrology/egae070.

Blatter, D.L., Sisson, T.W., Hankins, W.Ben, 2023. Garnet stability in arc basalt, andesite, and dacite—an experimental study. Contrib. Mineral. Petrol. 178, 33. https://doi.org/10.1007/s00410-023-02008-w.

Blum-Oeste, M., Wörner, G., 2016. Central Andean magmatism can be constrained by three ubiquitous end-members. Terra Nov 28, 434–440. https://doi.org/10.1111/ter.12237.

Borghini, G., Fumagalli, P., 2020. Melting relations of anhydrous olivine-free pyroxenite Px1 at 2 GPa. Eur. J. Miner. 32, 251–264. https://doi.org/10.5194/ejm-32-251-2020.

Bowman, E.E., Ducea, M.N., 2023. Pyroxenite melting at subduction zones. Geology. 51, 383–386. https://doi.org/10.1130/G50929.1.

Bowman, E.E., Ducea, M.N., Triantafyllou, A., 2021. Arclogites in the subarc lower crust: effects of crystallization, partial melting, and retained melt on the foundering ability of residual roots. J. Petrol. 62, egab094. https://doi.org/10.1093/petrology/egab094.

Braunger, S., Marks, M.A.W., Wenzel, T., Chmyz, L., Guitarrari Azzone, R., Markl, G., 2020. Do carbonatites and alkaline rocks reflect variable redox conditions in their upper mantle source? Earth Planet. Sci. Lett. 533, 116041 https://doi.org/10.1016/j.epsl.2019.116041.

Chakhmouradian, A.R., Zaitsev, A.N., 2012. Rare earth mineralization in igneous rocks: sources and processes. Elements 8, 347–353. https://doi.org/10.2113/gselements.8.5.347.

Depine, G.V., Andronicos, C.L., Phipps-Morgan, J., 2008. Near-isothermal conditions in the middle and lower crust induced by melt migration. Nature 452, 80–83. https://doi.org/10.1038/nature06689.

Dhuime, B., Bosch, D., Bodinier, J.-L., Garrido, C.J., Bruguier, O., Hussain, S.S., Dawood, H., 2007. Multistage evolution of the Jijal ultramafic–mafic complex (Kohistan, N Pakistan): implications for building the roots of island arcs. Earth Planet. Sci. Lett. 261, 179–200. https://doi.org/10.1016/j.epsl.2007.06.026.

Ducea, M.N., 2002. Constraints on the bulk composition and root foundering rates of continental arcs: a California arc perspective. J. Geophys. Res. Solid Earth 107, 2304. https://doi.org/10.1029/2001jb000643.

Ducea, M.N., Barton, M.D., 2007. Igniting flare-up events in Cordilleran arcs. Geology 35, 1047–1050. https://doi.org/10.1130/G23898A.1.

Ducea, M.N., Chapman, A.D., Bowman, E., Balica, C., 2021b. Arclogites and their role in continental evolution; part 2: relationship to batholiths and volcanoes, density and foundering, remelting and long-term storage in the mantle. Earth-Sci. Rev. 214, 103476 https://doi.org/10.1016/j.earscirev.2020.103476.

Ducea, M.N., Chapman, A.D., Bowman, E., Triantafyllou, A., 2021a. Arclogites and their role in continental evolution; part 1: background, locations, petrography, geochemistry, chronology and thermobarometry. Earth-Sci. Rev. 214, 103375 https://doi.org/10.1016/j.earscirev.2020.103375.

Ducea, M.N., Seclaman, A.C., Murray, K.E., Jianu, D., Schoenbohm, L.M., 2013. Mantle-drip magmatism beneath the Altiplano-Puna plateau, central Andes. Geology. 41, 915–918. https://doi.org/10.1130/G34509.1.

Elkins-Tanton, L.T., 2007. Continental magmatism, volatile recycling, and a heterogeneous mantle caused by lithospheric gravitational instabilities. J. Geophys. Res. Solid Earth 112, 1–13. https://doi.org/10.1029/2005JB004072.

Furman, T., Nelson, W.R., Elkins-Tanton, L.T., 2016. Evolution of the East African rift: drip magmatism, lithospheric thinning and mafic volcanism. Geochim. Cosmochim. Acta 185, 418–434. https://doi.org/10.1016/j.gca.2016.03.024.

Gaetani, G.A., Grove, T.L., 1998. The influence of water on melting of mantle peridotite. Contrib. Mineral. Petrol. 131, 323–346. https://doi.org/10.1007/s004100050396.

Goodenough, K.M., Deady, E.A., Beard, C.D., Broom-Fendley, S., Elliott, H.A.L., van den Berg, F., Öztürk, H., 2021. Carbonatites and Alkaline Igneous Rocks in Post-Collisional Settings: storehouses of Rare Earth Elements. J. Earth Sci. 32, 1332–1358. https://doi.org/10.1007/s12583-021-1500-5.

Goodenough, K.M., Schilling, J., Jonsson, E., Kalvig, P., Charles, N., Tuduri, J., Deady, E. A., Sadeghi, M., Schiellerup, H., Müller, A., Bertrand, G., Arvanitidis, N., Eliopoulos, D.G., Shaw, R.A., Thrane, K., Keulen, N., 2016. Europe's rare earth element resource potential: an overview of REE metallogenetic provinces and their geodynamic setting. Ore Geol. Rev. 72, 838–856. https://doi.org/10.1016/j.oregeorev.2015.09.019.

Green, T.H., Blundy, J.D., Adam, J., Yaxley, G.M., 2000. SIMS determination of trace element partition coefficients between garnet, clinopyroxene and hydrous basaltic liquids at 2–7.5 GPa and 1080–1200°C. Lithos. 53, 165–187. https://doi.org/10.1016/S0024-4937(00)00023-2.

Grove, T.L., Till, C.B., Krawczynski, M.J., 2012. The role of H2O in subduction zone magmatism. Annu. Rev. Earth Planet. Sci. 40, 413–439. https://doi.org/10.1146/annurev-earth-042711-105310.

Hirschmann, M.M., 2000. Mantle solidus: experimental constraints and the effects of peridotite composition. Geochem. Geophys. Geosyst. 1 https://doi.org/10.1029/2000GC000070, 2000GC000070.

Hirschmann, M.M., Kogiso, T., Baker, M.B., Stolper, E.M., 2003. Alkalic magmas generated by partial melting of garnet pyroxenite. Geology. 31, 481–484. https://doi.org/10.1130/0091-7613(2003)031<0481:AMGBPM>2.0.CO;2.

Holwell, D.A., Fiorentini, M.L., Knott, T.R., McDonald, I., Blanks, D.E., Campbell McCuaig, T., Gorczyk, W., 2022. Mobilisation of deep crustal sulfide melts as a first order control on upper lithospheric metallogeny. Nat. Commun. 13, 573. https://doi.org/10.1038/s41467-022-28275-y.

Hutchison, W., Finch, A.A., Borst, A.M., Marks, M.A.W., Upton, B.G.J., Zerkle, A.L., Stüeken, E.E., Boyce, A.J., 2021. Mantle sources and magma evolution in Europe's largest rare earth element belt (Gardar Province, SW Greenland): new insights from sulfur isotopes. Earth Planet. Sci. Lett. 568, 117034 https://doi.org/10.1016/j.epsl.2021.117034.

Jackson, M.D., Blundy, J., Sparks, R.S.J., 2018. Chemical differentiation, cold storage and remobilization of magma in the Earth's crust. Nature 564, 405–409. https://doi.org/10.1038/s41586-018-0746-2.

Kägi, R., Müntener, O., Ulmer, P., Ottolini, L., 2005. Piston-cylinder experiments on H2O undersaturated Fe-bearing systems: an experimental setup approaching fO2 conditions of natural calc-alkaline magmas. Am. Mineral. 90, 708–717. https://doi.org/10.2138/am.2005.1663.

Kara, J., Väisänen, M., Heinonen, J.S., Lahaye, Y., O'Brien, H., Huhma, H., 2020. Tracing arclogites in the Paleoproterozoic Era – a shift from 1.88 Ga calc-alkaline to 1.86 Ga high-Nb and adakite-like magmatism in central Fennoscandian Shield. Lithos. 372–373, 105663 https://doi.org/10.1016/j.lithos.2020.105663.

Kelemen, P.B., Rilling, J.L., Parmentier, E.M., Mehl, L., Hacker, B.R., 2004. Thermal structure due to solid-state flow in the mantle wedge beneath arcs, in: Eiler, J. (Ed.), Inside the Subduction Factory, Volume 138. American Geophysical Union, Washington, D.C., pp. 293–311. https://doi.org/10.1029/138GM13.

Keshav, S., Gudfinnsson, G.H., Sen, G., Fei, Y., 2004. High-pressure melting experiments on garnet clinopyroxenite and the alkalic to tholeiitic transition in ocean-island basalts. Earth Planet. Sci. Lett. 223, 365–379. https://doi.org/10.1016/j.epsl.2004.04.029.

Kogiso, T., Hirschmann, M.M., 2006. Partial melting experiments of bimineralic eclogite and the role of recycled mafic oceanic crust in the genesis of ocean island basalts. Earth Planet. Sci. Lett. 249, 188–199. https://doi.org/10.1016/j.epsl.2006.07.016.

Kogiso, T., Hirschmann, M.M., Frost, D.J., 2003. High-pressure partial melting of garnet pyroxenite: possible mafic lithologies in the source of ocean island basalts. Earth Planet. Sci. Lett. 216, 603–617. https://doi.org/10.1016/S0012-821X(03)00538-7.

Kogiso, T., Hirschmann, M.M., Pertermann, M., 2004. High-pressure Partial Melting of Mafic Lithologies in the Mantle. J. Petrol. 45, 2407–2422. https://doi.org/10.1093/petrology/egh057.

Lambart, S., Baker, M.B., Stolper, E.M., 2016. The role of pyroxenite in basalt genesis: melt-PX, a melting parameterization for mantle pyroxenites between 0.9 and 5 GPa. J. Geophys. Res. Solid Earth 121, 5708–5735. https://doi.org/10.1002/2015JB012762.

Lambart, S., Laporte, D., Provost, A., Schiano, P., 2012. Fate of pyroxenite-derived melts in the peridotitic mantle: thermodynamic and experimental constraints. J. Petrol. 53, 451–476. https://doi.org/10.1093/petrology/egr068.

Lambart, S., Laporte, D., Schiano, P., 2013. Markers of the pyroxenite contribution in the major-element compositions of oceanic basalts: review of the experimental constraints. Lithos. 160–161, 14–36. https://doi.org/10.1016/j.lithos.2012.11.018.

Lee, C.-T.A., 2014. Physics and Chemistry of Deep Continental Crust Recycling, in: Holland, H.D., Turekian, K.K. (Eds.), Treatise On Geochemistry: Second Edition. Elsevier, Oxford, pp. 423–456. https://doi.org/10.1016/B978-0-08-095975-7.00314-4.

Lee, C.T.A., Cheng, X., Horodyskyj, U., 2006. The development and refinement of continental arcs by primary basaltic magmatism, garnet pyroxenite accumulation, basaltic recharge and delamination: insights from the Sierra Nevada, California. Contrib. Mineral. Petrol. 151, 222–242. https://doi.org/10.1007/s00410-005-0056-1.

Le Roux, V., Dasgupta, R., Lee, C.-T.A., 2011. Mineralogical heterogeneities in the Earth's mantle: constraints from Mn, Co, Ni and Zn partitioning during partial melting. Earth Planet. Sci. Lett. 307, 395–408. https://doi.org/10.1016/j.epsl.2011.05.014.

Le Roux, V., Lee, C.-T.A., Turner, S.J., 2010. Zn/Fe systematics in mafic and ultramafic systems: implications for detecting major element heterogeneities in the Earth's mantle. Geochim. Cosmochim. Acta 74, 2779–2796. https://doi.org/10.1016/j.gca.2010.02.004.

Loucks, R.R., 2021. Deep entrapment of buoyant magmas by orogenic tectonic stress: its role in producing continental crust, adakites, and porphyry copper deposits. Earth-Sci. Rev. 220, 103744 https://doi.org/10.1016/j.earscirev.2021.103744.

Mallik, A., Lambart, S., Chin, E.J., 2021. Tracking the Evolution of Magmas from Heterogeneous Mantle Sources to Eruption, in: Marquardt, H., Ballmer, M., Cottaar, S., Konter, J. (Eds.), Mantle Convection and Surface Expressions, Geophysical Monograph Series, New Jersey, pp. 151–177. https://doi.org/10.1002/9781119528609.ch6.

Marks, M.A.W., Markl, G., 2017. A global review on agpaitic rocks. Earth-Sci. Rev. 173, 229–258. https://doi.org/10.1016/j.earscirev.2017.06.002.

McDonough, W.F., Sun, S.-S., 1995. The composition of the Earth. Chem. Geol. 120, 223–253. https://doi.org/10.1016/0009-2541(94)00140-4.

Médard, E., Schmidt, M.W., Schiano, P., Ottolini, L., 2006. Melting of amphibole-bearing wehrlites: an experimental study on the origin of ultra-calcic nepheline-normative melts. J. Petrol. 47, 481–504. https://doi.org/10.1093/petrology/egi083.

Murray, K.E., Ducea, M.N., Schoenbohm, L., 2015. Foundering-driven lithospheric melting: the source of central Andean mafic lavas on the Puna Plateau (22°S-27°S), in: DeCelles, P.G., Ducea, M.N., Carrapa, B., and Kapp, P.A. (Eds.), Geodynamics of a Cordilleran Orogenic System: The Central Andes of Argentina and Northern Chile. The Geological Society of America, Colorado, pp. 139–166. https://doi.org/10.1130/2015.1212(08).

O'Neill, H.S.C., Wall, V.J., 1987. The olivine—orthopyroxene—spinel oxygen geobarometer, the nickel precipitation curve, and the oxygen fugacity of the earth's upper mantle. J. Petrol. 28, 1169–1191. https://doi.org/10.1093/petrology/28.6.1169.

Pál-Molnár, E., Batki, A., Almási, E., Kiss, B., Upton, B.G.J., Markl, G., Odling, N., Harangi, S., 2015. Origin of mafic and ultramafic cumulates from the Ditrău Alkaline Massif. Romania. Lithos 239, 1–18. https://doi.org/10.1016/j.lithos.2015.09.022.

Pertermann, M., Hirschmann, M.M., 2003. Anhydrous partial melting experiments on MORB-like eclogite: phase relations, phase compositions and mineral–melt partitioning of major elements at 2–3 GPa. J. Petrol. 44, 2173–2201. https://doi.org/10.1093/petrology/egg074.

Pertermann, M., Hirschmann, M.M., Hametner, K., Günther, D., Schmidt, M.W., 2004. Experimental determination of trace element partitioning between garnet and silica-rich liquid during anhydrous partial melting of MORB-like eclogite. Geochem. Geophys. Geosyst. 5, Q05A01. https://doi.org/10.1029/2003GC000638.

Schmidt, M.W., Jagoutz, O., 2017. The global systematics of primitive arc melts. Geochem. Geophys. Geosyst. 18, 2817–2854. https://doi.org/10.1002/2016GC006699.

Smith, M.P., Moore, K., Kavecsánszki, D., Finch, A.A., Kynicky, J., Wall, F., 2016. From mantle to critical zone: a review of large and giant sized deposits of the rare earth elements. Geosci. Front. 7, 315–334. https://doi.org/10.1016/j.gsf.2015.12.006.

Sorbadere, F., Médard, E., Laporte, D., Schiano, P., 2013. Experimental melting of hydrous peridotite–pyroxenite mixed sources: constraints on the genesis of silica-undersaturated magmas beneath volcanic arcs. Earth Planet. Sci. Lett. 384, 42–56. https://doi.org/10.1016/j.epsl.2013.09.026.

Syracuse, E.M., van Keken, P.E., Abers, G.A., 2010. The global range of subduction zone thermal models. Phys. Earth Planet. Inter. 183, 73–90. https://doi.org/10.1016/j.pepi.2010.02.004.

Tang, M., Erdman, M., Eldridge, G., Lee, C.-T.A., 2018. The redox "filter" beneath magmatic orogens and the formation of continental crust. Sci. Adv. 4 https://doi.org/10.1126/sciadv.aar4444 eaar4444.

Tang, M., Lee, C.-T.A., Chen, K., Erdman, M., Costin, G., Jiang, H., 2019. Nb/Ta systematics in arc magma differentiation and the role of arclogites in continent formation. Nat. Commun. 10, 235. https://doi.org/10.1038/s41467-018-08198-3.

Wall, F., 2014. Rare earth elements. In: Gunn, G. (Ed.), Critical Metals Handbook. John Wiley & Sons, West Sussex, pp. 312–339.

Wang, C., Jin, Z., Gao, S., Zhang, J., Zheng, S., 2010. Eclogite-melt/peridotite reaction: experimental constrains on the destruction mechanism of the North China Craton. Sci. China Earth Sci. 53, 797–809. https://doi.org/10.1007/s11430-010-3084-2.

Wilson, W.R., Houseman, G.A., Buiter, S.J.H., McCaffrey, K.J.W., Doré, A.G., 2019. Fifty years of the Wilson Cycle concept in plate tectonics: an overview. Geol. Soc. London, Spec. Publ. 470, 1–17. https://doi.org/10.1144/SP470-2019-58.

Zieman, L., Ibañez-Mejia, M., Rooney, A.D., Bloch, E., Pardo, N., Schoene, B., Szymanowski, D., 2023. To sink, or not to sink: the thermal and density structure of the modern northern Andean arc constrained by xenolith petrology. Geology 51, 586–590. https://doi.org/10.1130/G50973.1.